ELSEVIER

Contents lists available at ScienceDirect

Quaternary Science Advances

journal homepage: www.sciencedirect.com/journal/quaternary-science-advances



Spatiotemporal gravity changes at the Santorini Volcanic complex and their interpretation

Melissinos Paraskevas ^{a,*}, Demitris Paradissis ^a, Emilie Hooft ^b, Paraskevi Nomikou ^c

- ^a Dionysos Satellite Observatory, National Technical University of, Polytechneioupoli, Zografou, 15780, Athens, Greece
- ^b Department of Earth Sciences, University of Oregon, OR, 97403, Eugene, USA
- ^c Department of Geology and Geoenvironment, National and Kapodistrian University of Athens, Panepistimioupoli, Zografou, 15784, Athens, Greece

ARTICLE INFO

Keywords: Santorini Spatiotemporal gravity changes Magma source Volcano Greece Caldera

ABSTRACT

Understanding the complex dynamics of volcanic systems demands a multidimensional approach that combines geophysics, geology, and geodetics. In this study, we examine observed spatiotemporal gravity changes within the Santorini volcanic complex from 1975 to 2014. The historical data indicates that gravity has been increasing continuously since at least 1966 until our latest measurements in 2014, albeit with a decreasing rate of increase over time. Utilizing gravity inversion of various gravity datasets and evidence from other studies, we explore different scenarios to shed light on the underlying processes. Our preferred interpretation involves both a magmatic episode and continuous evolution of the shallow structure. We find that the 2011-12 unrest period resulted from the intrusion of $\sim 3.3 \times 10^{11}$ kg of basaltic magma at 3 km depth near the previously identified Mogi source. We attribute the continuous gravity increase beneath Nea Kameni to a density increases at about 1350 m depth. We infer these are a result of hydrothermal fluctuations, degassing, and/or vesicle collapse within the stored magma.

Units: $1 \text{mGal} = 10^{-5} \text{ m/s}^2$ (SI)

1. Introduction

Santorini is located in the central part of the Hellenic Volcanic Arc (South Aegean Sea) and is well known for the Late Bronze Age "Minoan" eruption that might have been responsible for the decline of the great Minoan civilization on the island of Crete. Santorini has evolved over at least 650,000 years. The "Minoan" eruption was the last Plinian eruption of Santorini Island (Sparks and Wilson, 1990; Druitt et al., 1999; Druitt, 2014; Cadoux et al., 2014; Johnston et al., 2014), discharging 34.5 \pm 6.8 km³ dense-rock equivalent (DRE) of silicic magma and rock fragments (Karstens et al., 2023), mostly in the form of pyroclastic flows that entered the sea and were preserved as ignimbrite in the surrounding submarine basins (Sigurdsson et al., 2006).

Subsequent eruptions formed the Kameni complex at the center of Santorini's caldera, the result of a sub-aerial extrusion of $4.3\pm0.7~{\rm km}^3$ intra-caldera shield, forming a 3.5 km basal diameter, the summit of which towers up 470 m above the caldera floor. The total dense-rock equivalent volume of products from Kameni Volcano is $4.85\pm0.7~{\rm km}^3$ (Nomikou et al., 2014). Vents lie within a 600-m-wide

NE-SW-trending zone, the Kameni line, which reflects the fault control on magma ascent (Pyle and Elliott, 2006; Heath et al., 2020). Nine sub-aerial, largely effusive eruptions have been reported or inferred from historic records: 197 BCE, AD 46-47, AD 726, 1570/1573, 1707-1711, 1866-70, 1925-28, 1939-41, and 1950(Nomikou et al., 2014). Recent bathymetric research of the Kameni edifice has revealed previously unknown, submarine lava flows and submarine extensions of known sub-aerial ones, together with the surrounding pyroclastic apron.

Santorini is characterized by a complex geological structure and evolution. Despite its relatively small area, a large number of geological formations, aged from the Upper Triassic to the present day, participate in its structure. The oldest rocks are found only in the southeastern part of the island (Chatzis et al., 2022). These limestone rocks formed a pre-volcanic small island. Numerous volcanic formations, products of the volcanic activity, occupy most of the island complex of Santorini (Fig. 1).

In January 2011, Santorini entered a phase of unrest that persisted until March 2012 (Parks et al., 2012, 2015), without any eruptive activity. The unrest phase was characterized by a large number of

E-mail addresses: melipara1@mail.ntua.gr (M. Paraskevas), dempar@central.ntua.gr (D. Paradissis), emilie@uoregon.edu (E. Hooft), evinom@geol.uoa.gr (P. Nomikou).

^{*} Corresponding author.

minor-magnitude (M < 3.3) volcanotectonic earthquakes occurring at depths of 1 to 6 kilometers along a nearly vertical plane, 6 km in length along the Kameni line (Newman et al., 2012). The increased seismicity was accompanied by up to 10 cm of inflation on Nea Kameni Island measured by ground-based GNSS and satellite radar interferometry, which corresponds to an injection of about 10-20 million m³ of magma at 3-6 km beneath the caldera (Newman et al., 2012; Parks et al., 2012, 2015; Papoutsis et al., 2013; Foumelis et al., 2013). Small increases in the fluxes of H_2 and mantle-derived CO_2 were also recorded during the unrest period (Parks et al., 2013; Tassi et al., 2013).

Another effective geophysical methodology for volcano monitoring involves conducting onshore measurements of the gravitational field, specifically by comparing gravity data obtained during different time intervals. The Dionysos Satellite Observatory of the National Technical University of Athens (DSO/NTUA) possesses a dataset of gravity measurements taken on Santorini Island dating back to 1976 (Agatza –Balodimou and Papazissi, 1984). In early December 2012, a dataset of gravity measurements was conducted at specific locations within the Santorini volcanic group. Subsequently, this dataset was complemented and finalized in September 2014 (Paraskevas et al., 2014, 2019, 2021).

The processing of the aforementioned data was carried out using Geographic Information Systems (GIS). Additionally, remote sensing (RS) techniques were applied at various stages of data processing (Sonker and Tripathi, 2022; Taloor et al., 2023). An illustrative example

involves the determination of temporal elevation changes at gravity benchmarks achieved through ground-based measurements, Global Navigation Satellite System (GNSS) measurements, and Interferometric Synthetic Aperture Radar (InSAR) data. This methodology highlights the significance of utilizing a combination of tools and techniques (GIS and RS) to enhance the effective utilization of gravity data (Taloor et al., 2021, 2022).

This paper is the first to analyze temporal gravity variations at the Santorini volcanic group, using data collected from Thira, Thirassia, Palea and Nea Kameni, and Aspronisi. The main purpose is to understand alterations within the upper volcanic system both in relation to the 2011-2012 unrest period and during the pre- and post-unrest periods.

2. Data and methods

2.1. Gravity datasets

Since the 1950s, microgravity surveys have been utilized to measure changes in subsurface mass and/or density prior to volcanic eruptions on various time scales (Yokoyama and Tajima, 1957). This process involves conducting a series of measurements at different points that encompass the entire area of interest. Subsequently, the entire survey is repeated after a span of months or years, allowing for the determination of temporal changes in gravity.

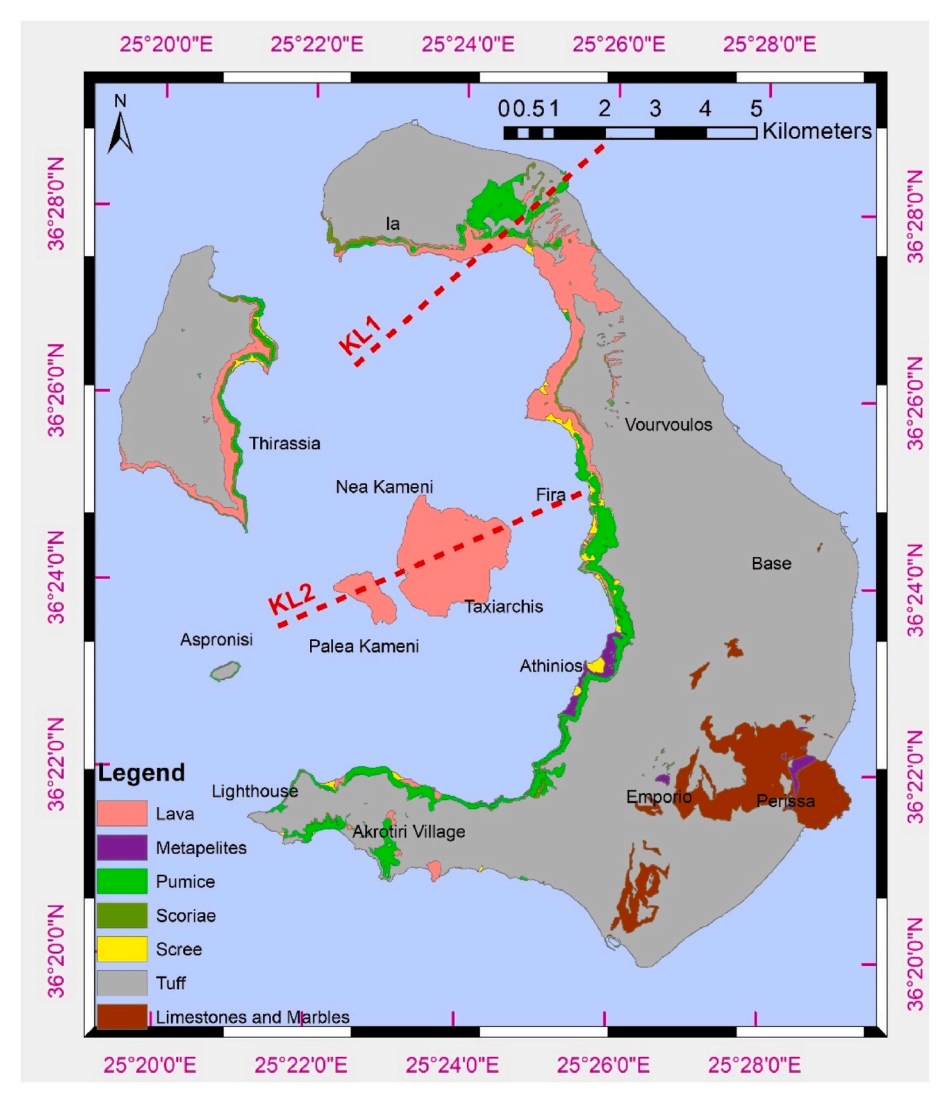


Fig. 1. Simplified geologic map of the Santorini volcanic complex (modified from Druitt, 2014). Red dashed lines indicate Kolumbo (KL1) and Kameni (KL2) Lines.

In this research on the Santorini volcanic complex, several datasets spanning from 1966 to 2014 were compiled, as described in Paraskevas et al. (2021). These datasets were standardized to a common gravity datum and corrected for factors such as solid earth and ocean-loading tides, instrumental drift, calibration, and atmospheric variations. The gravity datasets utilized in this investigation include:

- a. Raw gravity measurements provided by the Hellenic Military Geographical Service (HMGS) using three Lacoste and Roberg gravimeters simultaneously that were made in 1966, 1968, and 1975 (Paraskevas et al., 2022, 2023).
- b. Gravity Survey of 1976 (Paraskevas et al., 2019, 2021; Agatza-Balodhmou and Papazissi, 1984) that was executed by the National Technical University/Dionysus Satellite Observatory (NTUA/DSO) using Lacoste and Roberg gravimeters.
- c. Gravity Survey of 2012 (Paraskevas et al., 2019, 2021), executed by NTUA/DSO in 2012 and collected using a Scintrex CG5 gravimeter.
- d. Gravity Survey of 2014 (Paraskevas et al., 2019, 2021), executed by NTUA/DSO in 2014 and collected using a Scintrex CG5 gravimeter.
- e. Repeated gravity measurements of 1981, 1984, 1986, 1988, 1998, 2001, and 2005 to first-order National gravity network station provided by HMGS (Paraskevas et al., 2021, 2022, 2023).

These datasets were integrated into a Geographic Information System (GIS), facilitating their systematic organization, comparison, modeling, and visualization. To enable this integration, dedicated databases were established to support subsequent data manipulation (Paraskevas et al., 2021). The common stations of the gravity surveys have been summarized in Table 1 and are visually depicted in Fig. 2.).

2.2. Elevation changes over time

Elevation changes over time have a significant impact on gravity. Parks et al. (2012) argued that there were no significant elevation differences at the triangulation points from the existing raw geodetic measurements in Santorini between 1955 and 1985. However, by employing raw trigonometric observations from one station to another and utilizing one reference station near Emporio (not the adjusted elevations of four fixed stations), we find significant subsidence of the triangulation point at Nea Kameni of 9 cm (mean annual rate of 3 mm/year between 1955 and 1985). Meanwhile, the differences in elevation range from 0 to 4 cm for the remaining sites. The uncertainty of these measurements may influence the results because the mean standard deviation (std) of calculated elevations is 2-3 cm.

Using InSAR data, subsidence with an annual rate of about 5-6 \mbox{mm}

per year was also recorded at Nea Kameni Island from 1992 to 2010 (Lagios et al., 2013; Foumelis et al., 2013). Then the subsidence increased in the vicinity of Nea Kameni until January 2011 (Foumelis et al., 2013). A significant inflation was observed during the unrest period of 2011-2012 (Lagios et al., 2013; Foumelis et al., 2013; Papoutsis et al., 2013). After that period, the area returned to subsidence until 2017 (Papageorgiou et al., 2019). The estimated temporal variation in the elevation of each station was calculated using GIS, into which all the aforementioned datasets were incorporated. The summarized outcomes are presented in Table 1.

For this dataset the precision of the deformation estimations is limited. An exception to this limitation is the well-documented inflation during the period 2011-2012, for which numerous studies provide specific values of inflation.

2.3. Theoretical background

In volcano monitoring studies temporal gravity changes are typically divided into two groups of effects: non-volcanic gravity effects and volcanic-origin gravity effects.

2.3.1. Non-volcanic (or permanent) gravity effects

These effects arise from various phenomena, including Earth and ocean tides, atmospheric and hydrological influences, instrumental discrepancies, Earth's polar motion etc. To calculate the final absolute gravity values or relative values to a reference station, these factors were either added to, or subtracted from, the measurements. Notably, the most prominent signal in the observed gravity data arises from Earth's tides and instrument drift. For the measurements used in this study, corrections for Earth and ocean tides, atmospheric pressure, and instrument drift were applied as detailed in Paraskevas et al. (2021). This ensures that the gravity values analyzed are accurately corrected for non-volcanic effects, enabling a more precise evaluation of volcanic-related variations.

Local effects in the vicinity of the stations can also contribute to observed gravity changes (Torge, 1989). During the time period studies there were human constructions in the vicinity of stations in Athinios, Perissa, Fira, Vourvoulos, Lighthouse, and Emporio (Fig. 2). Furthermore, stations at Athinios, Nea and Palea Kameni, Fira, and Aspronisi are located at ports or on the coast and so seasonal or long-term changes in sea level may affect the gravity measurements. Significant changes at tide gauges in the area were reported during the unrest period of 2011-2012 (Panagiotopoulos et al., 2015), which could also affect gravity changes, and perhaps they were underestimated as permanent gravity effects (mostly related to ocean tide phenomena that can be

Table 1 Gravity and height changes at common stations measured in 1975 or 1976 and 2012 or 2014. $\Delta g_{observed}$, is from Paraskevas et al. (2021) and the estimated height changes, dh, are from Lagios et al. (2013), Foumelis et al., (2013), Papoutsis et al. (2013); and Papageorgiou et al., 2019. The time interval is given by dyear. The standard deviation (std) of $\Delta g_{observed}$ was recalculated to account for unmodeled local phenomena as described in the text. The FAG was used to calculate the gravity change residuals, $\Delta g_{residual}$, using equations (3) and (4).

Stations	Lat	Long	Elev	dyear	$\Delta g_{\rm obs}$	Std	dh	FAG	Δg_{res}
(units)	°N	°E	m		mGal	mGal	m	mGal	mGal
Nea Kameni Port	36.411	25.400	1.465	2014-1976	0.255	0.041	-0.048	-0.015	0.240
Nea Kameni middle	36.410	25.401	2.010	2014-1975	0.246	0.052	-0.055	-0.017	0.229
Center of Nea Kameni	36.405	25.395	126.737	2012-1976	0.377	0.037	-0.086	-0.027	0.350
Taxiarrchs (N. Kameni)	36.400	25.405	2.962	2012-1976	0.282	0.035	-0.014	-0.004	0.278
Palaia Kameni	36.399	25.381	1.021	2012-1976	0.269	0.037	-0.019	-0.006	0.263
Athinios	36.387	25.431	1.596	2014-1976	0.067	0.030	-0.031	-0.010	0.057
Aspronisi	36.383	25.349	3.200	2012-1976	0.020	0.068	0.017	0.005	0.025
Base	36.407	25.479	34.610	2014-1984	0.015	0.014	-0.015	-0.005	0.010
Emporio	36.357	25.445	76.548	2014-1976	-0.009	0.042	0.029	0.009	0.000
Vourvoulos	36.435	25.436	123.537	2014-1976	0.018	0.031	0.009	0.003	0.021
Perissa	36.357	25.474	4.400	2012-1975	0.029	0.030	-0.021	-0.006	0.023
Ia	36.461	25.390	155.730	2012-1975	0.057	0.032	-0.011	-0.003	0.054
Fira	36.418	25.428	1.140	2014-1968	0.062	0.039	0.015	0.005	0.067
Lighthouse	36.358	25.357	99.360	2014-1975	0.009	0.044	0.018	0.006	0.015

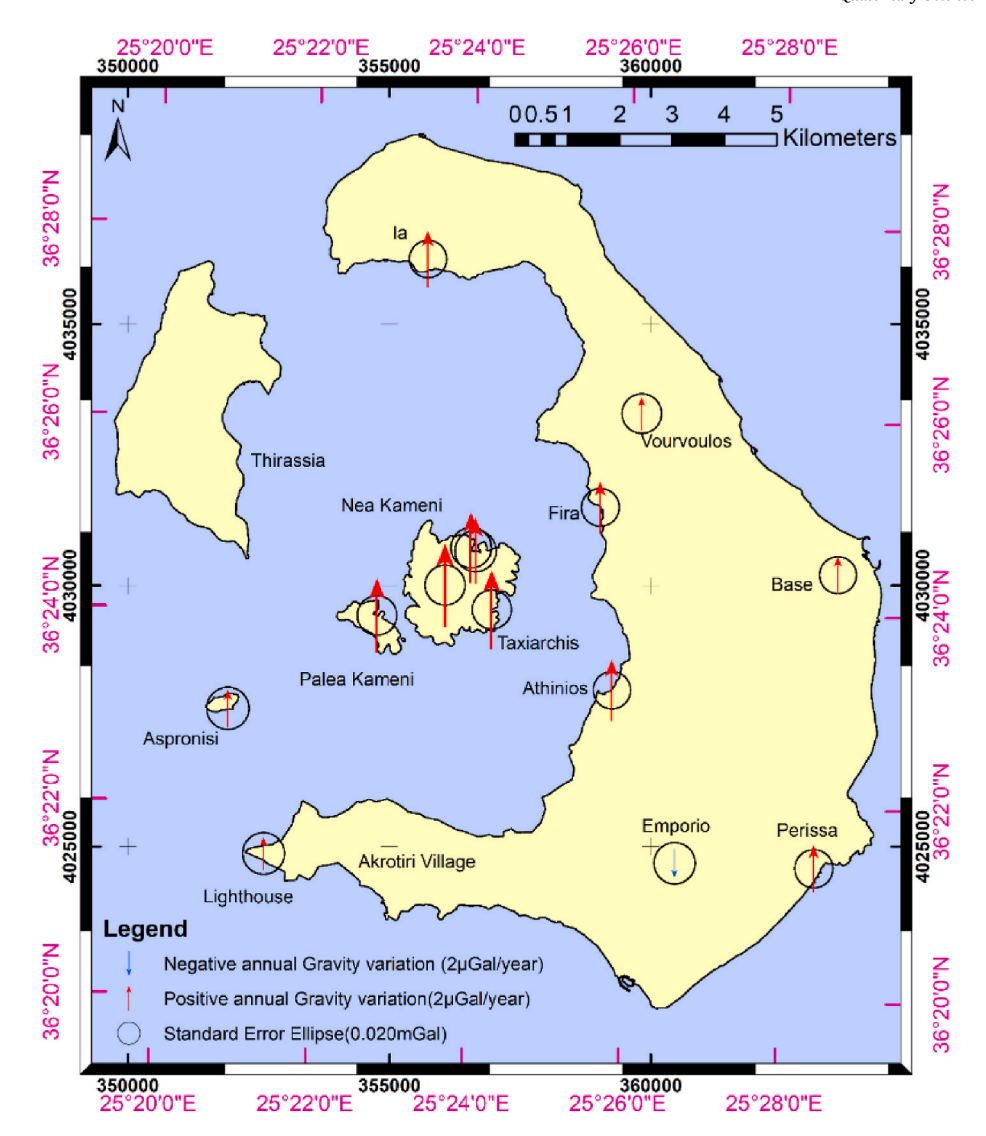


Fig. 2. Annual variations in gravity over time (Paraskevas et al., 2021).

locally underestimated when using global models). We do not have enough data to calculate the gravity effect of these local phenomena. Typical gravity variations due to sea level changes can be as large as 20 μ Gal/m of tidal change (Seigel, 1995), while the gravity effect of small buildings is up to 3-5 μ Gal (e.g., Loj and Porzucek, 2019). Consequently, we add 10 μ Gal to the standard deviation (std) of stations next to the sea and 5 μ Gal to stations next to human constructions.

A possible contribution to the recorded gravity variations is the effect of rainfall due to precipitation within the volcano during the period covered by the gravity surveys. The old measurements were taken during dry summers in 1975 and 1976 (0 mm of precipitation), while measurements in 2012 were taken in rainy December of 2012 (46.4 mm monthly rainfall) and in September of 2014 (0.4 mm monthly rainfall). As the hydrological structure around our stations is not well known, and there are no available data or measurements for an unconfined aquifer in the Santorini area, we estimate the maximum rainfall effect on gravity (DgRmax) using (Seigel, 1995; Torge, 1989):

$$Dg_{Rmax} = 0.04192d \text{ mGal/m} \tag{1}$$

Where d represents the rainfall at the station for a representative time period. Rainfall data were obtained from the Hellenic National Meteorological Service using the Santorini weather station (Elevation: 183 m, Latitude: 36°24′ N, Longitude: 25° 24′ E) (HNMS, 2020). The rainfall data from www.emy.gr indicate that the maximum effect on

measurements, using Equation (1), was 3 μ Gal Finally, we could also correct our gravity signal for seasonal hydrologic variations of $\pm 5~\mu$ Gal (higher in summer and lower in winter) (Okubo et al., 2013; Naujoks et al., 2010). Since both these values are very small compared with the standard deviation (std) of the measurements we do not correct for these effects.

Remaining hydrological effects, such as water table fluctuations and changes in water-mass storage above the water table, within the unsaturated (vadose) zone, are not treated as corrections. They remain in the residual gravity changes and are part of the subject of inversion and interpretation, in other words these types of hydrological variations are considered as part of the sought sources.

2.3.2. Volcanic origin gravity effects

These effects are used to investigate changes in final gravity values (referred to the National Gravity Network) that have been corrected for permanent, non-volcanic gravity effects. First, changes in the elevation of a benchmark due to deformation of the Earth's crust in its vicinity usually causes measurable gravity effects. The calculated gravity effect, based on the magnitude of inflation or deflation, must be subtracted from the observed gravity changes. During the deformation, the gravity station (benchmark) is vertically displaced along with the topographic surface. To investigate gravity changes imposed by the vertical displacement of the topographic surface, such as inflation or subsidence,

every benchmark was moved vertically from its measured position on the pre-deformation topographic surface to its new post-deformation position in the ambient gravity field (Vajda et al., 2016).

The gravity changes are also caused by the gravitational effect of subsurface deformations (e.g., Fernández and Rundle, 1994; Bonafede and Mazzanti, 1999; Battaglia et al., 2008; Vajda et al., 2019; Currenti, 2014). However, unlike the surface vertical displacements, these deformations are not directly observable, so their effect cannot be computed and applied as a correction to the gravity changes, but only estimated or modeled. The application of all the above corrections to the gravity changes results in the residual gravity changes that are used as input data in the inversion process.

To investigate this process, we must invert residual gravity, to find the source of the anomaly. There are several analytical models (sphere, ellipsoid, sill, dyke, cylinder etc) or numerical models (FEM, BEM) that can be employed to study the slow, long-term deformation at central volcanoes and calderas due to the pressurization of magma or hydrothermal reservoirs at depth. These models can be numerical calculated by inverting geodetic data or joint geodetic and InSAR observations. Gravity changes before and after deformation can also be modeled from joint GPS, InSAR, and gravity observations (Battaglia et al., 2008).

The most common source geometry used to study residual gravity approximates the pressurized magma reservoir as a spherical body (Mogi, 1958). The gravitational attraction of a spherical body of finite size and mass, is identical to that of a point source with the same mass (Battaglia and Hill, 2009). The spherical shape requires a minimum number of model parameters and was used so as not to over-interpret the relatively sparse available data. Although a point source does not accurately represent the volcanic activity, it is computationally straightforward and actually fits real data quite well in many cases (Battaglia et al., 2008). The gravity effect of a Mogi–type (Mogi, 1958) magma reservoir is given by (Eggers, 1987):

$$\Delta g = \left(\frac{\Delta M_m G z}{\left(x^2 + z^2\right)^{\frac{3}{2}}}\right) \left[\ln m/s^2\right] \tag{2}$$

Where the mass $\Delta M_m=\rho\Delta V$, with ρ the density of the mass and ΔV the change in volume, G is the Universal Gravitational constant (6.674 x 10^{-11} N m^2 kg $^{-2}$), x is the horizontal surface distance (m) from the center of the Mogi source, and z is the depth (m) to the Mogi point source. Note that in equation (2) we have neglected the gravity effect due to the deformation and the propagation of density boundaries, which for the case of an isotropic source situated in a homogenous half-space is zero (Walsh and Rice, 1979).

We also validated and refined the constraints inferred from the Mogi models, by using an inversion approach known as Growth that involves the exploration of a broader set of models with a free geometry and subsurface cell population (Camacho et al., 2011, 2021). In applying this software, we concentrate on inversion approaches that make no a priori assumptions about the number or shapes of the source bodies sought (Vajda et al., 2022). The Growth iterative inversion procedure is based on minimizing the misfit between observed and model gravity data constrained by minimizing the total subsurface temporal mass change (Berrino et al., 2022). The GROWTH-dg tool supports inverse-modeling as well as a stand-alone quantity and it has several inversion parameters that lead to numerous solutions as described in detail by Camacho et al. (2021), Vajda et al. (2022), and Berrino et al. (2022).

3. Results

3.1. Numerical modelling

In this paper we invert gravity change residuals, $\Delta g_{residual}$, that are defined to focus on the volcanic process by correcting the observed gravity values for both the permanent, non-volcanic effects and the effects of topographic displacements:

$$\Delta g_{\text{residual}} = \Delta g_{\text{observed}} - \Delta g_{\text{DITE}} \tag{3}$$

Where $\Delta g_{observed}$ is the observed temporal gravity change at one station corrected for permanent gravity effects as described at section 2.3.1. Δg_{DITE} is the Deformation-Induced Topographic Effect (DITE) (Vajda et al., 2019). Δg_{DITE} is the sum of the gravity effect due to the vertical displacement of the gravity benchmark in the ambient gravity field and the attraction of topographic masses enclosed between the pre-and post-deformation topographic surface. (In this research we neglect the effect of surface mass changes because there are no reported volcanic fall-out products). Δg_{DITE} can be estimated through various methods, as discussed in Vajda et al. (2019, 2021). In this study, we use the normal free air gradient (FAG), a choice made by several other researchers. (e.g. Battaglia et al., 2003; Bagnardi et al., 2014):

$$\Delta g_{DITE} \approx FAG = -\gamma \Delta H \tag{4}$$

Where γ is the free-air gradient (the theoretical gradient $\gamma = -0.3086$ mGal/m), and ΔH is the vertical surface displacement (positive for relative uplift and negative for relative subsidence).

The results of the calculations are detailed in Table 1.

3.2. Total mass variation

Determining the total mass involved in a redistribution process is independent of any assumptions about the shape, density change, or depth of the source body. The fundamental approach to this calculation involves Gaussian surface integration of the residual anomaly across the measurement area (Sharma, 1986). The formula for computing the total mass is (Grant and West, 1965):

$$M = \frac{1}{2\pi G} \iint \Delta g(x, y) dx dy = \frac{1}{2\pi G} \sum \Delta g \Delta S$$
 (5)

where Δ g is the mean anomaly (gravity variation) within a small area element Δ S (m²) and $\sum \Delta g \Delta S$ is the sum over the entire measurement area. It is noteworthy that, for the purpose of estimating the order of magnitude of the mass change, an interpolation of Δg_{res} is applied, and the value of each pixel exceeding 0 is multiplied by the area of the corresponding pixel (Carbone et al., 2003). Based on the analysis, the mean $\Delta g = 0.062$ mGal and $S = 182 \times 10^6$ m². Consequently, we calculate a total mass of M = 2.9 $\times 10^{11}$ kg. We obtain very similar results using pixel sizes ranging from 500 to 2000 m. This mass should be regarded as a minimum estimate, given that the anomaly is incomplete, and its determination is independent of the inner geometry of the encompassing body (Miller et al., 2017).

3.3. Modelling of gravity residuals

Initially, we will create Model 1, in which we will invert the residual gravity to find the source of the anomaly. Subsequently, we will construct Model 2, in which we will test whether the source identified by various other researchers using geodetic and remote sensing methods during the 2011-12 unrest can account for the residual gravity. The third model incorporates the combination of Models 1 and 2. In this model, we will consider the gravity effect from the 2011-12 unrest using data from other researchers and invert the remaining signal to identify possible other causes for the observed gravity variations.

3.3.1. Model 1: Single body mogi source

In first approximation we invert the residual gravity for the entire observation period to find the best-fitting Mogi source model. This Model 1 constrains the source location and associated mass variation using equation (2). We invert $\Delta g_{residual}$ from Table 1 using MATLAB's built-in fmin search function, which applies the Nelder-Mead method (Nelder and Mead, 1965), to perform an unconstrained nonlinear

minimization of the sum of the adjusted squared residuals. We tested 100 different initial values of the model (covering the entire study area horizontally, depths from 500 to 8000 m and associated mass change from 10^{10} to 10^{12} kg) and used the solution with the smallest least square difference to $\Delta g_{residual}$:

$$\chi^{2} = \sum_{i}^{N} \frac{\left(\Delta g_{model}(i) - \Delta g_{residual(i)}\right)^{2}}{std_{(i)}^{2}} \quad for \ i = 1, 2, ... 14 \ and \ N = 14$$
 (6)

The best-fit model is presented in Table 2 and graphically in Figs. 3 and 4. The calculated mass from Table 2 agrees with the total mass calculated in Section 3.2.

In a more rigorous approximation, we employ the GROWTH-Dg tool (Camacho et al., 2021). Due to the sparsity and poor signal-to-noise ratio of the input gravity data, there are a relatively large suite of different inversion models that satisfy the input data almost equally well. The selected inversion model is presented in Fig. 5. The calculated source body could be interpreted as a volumetric domain affected by magma intrusion/injection (swarm of thin dykes or dykes and sills, or eventually an injected conjugated fault system) with a bulk density increase of 19.3 kg/m 3 , over the entire volume. This leads to an equivalent mass increase of 4.1×10^{11} kg at a mean depth of 2169 m. which is comparable to the Mogi-source model (Table 2), although the calculated Mass change exceeds this value. The extra mass computed by the Growth-Dg tool might be attributed to the model's overfitting to the observed gravity residuals.

The calculated position of the Mogi point source and the volume of the GROWTH-dg solution are consistent with models proposed by other researchers (Foumelis et al., 2013; Papageorgiou et al., 2019; Saltogianni et al., 2014). These studies suggested Mogi point sources of deflation beneath Nea Kameni using InSar and GNSS data. According to their findings, this deflationary point remains stable both before and after the unrest period of 2011-2012, closely aligned with the position derived from the calculations in Table 2.

While the majority of the observed gravity changes can be explained by Model 1, the analytical approach struggles to account for variations in gravity at station Ia. In addition, the GROWTH-dg solution indicates the presence of an anomalous volume north of Nea Kameni. This location is close to the Mogi point sources calculated by several researchers for the period of unrest in 2011-2012. In the next section we seek a more suitable model that addresses this discrepancy.

3.3.2. Model 2: Single body at the location of the 2011-2012 unrest

The only significant unrest period since the last eruption in 1950 was during the 2011-12 unrest (Parks et al., 2013). Significant volume changes were calculated during this volcanic episode. Modeled locations of the Mogi point source were calculated using geodetic data by several researchers (Newman et al., 2012; Parks et al., 2012, 2015; Papoutsis et al., 2013; Foumelis et al., 2013) and typically agree to approximately 500 m. This yielded a median longitude, latitude, and depth for the source of 25.389°E, 36.426°N, and 4 km, respectively (Parks et al., 2015), with an estimated volume change of $1.4 - 2.1 \times 10^7$ m³ (Newman et al., 2012; Parks et al., 2012, 2015). Due to the lack of gravity measurements shortly before the unrest period of 2011-2012, gravity data cannot be included in a new GPS and InSAR joint calculation of a Mogi point source for this period. However, it remains valuable to construct Model 2, where the location and volume were fixed to the values

determined from the geodetic and remote sensing data (Newman et al., 2012; Parks et al., 2012, 2015; Papoutsis et al., 2013; Foumelis et al., 2013). This allows us to ascertain whether the 2011-2012 Mogi-source can account for the observed variations in gravity.

The volume increase during the 2011-2012 unrest episode could have been caused by the intrusion of magma, gas, or a mixture of the two (Druitt et al., 2019). The maximum gravity effects occur assuming magma intrusion at the modeled location. To determine the volume of magma intruded (ΔV_m), we take magma and reservoir compressibility into account (Mastin, 2007; Battaglia et al., 2008; Anderson and Segall, 2011):

$$\Delta V_m = \Delta V \left(1 + \frac{\beta_m}{\beta_L} \right) \tag{7}$$

where ΔV_i is the volume change from the inversion of deformation (geodetic volume), β_m is the magma compressibility, and β_c is the reservoir compressibility. Using a typical shallow-crustal compressibility of $3\times 10^{-11}~Pa^{-1}$ and a magma compressibility of $1.25\times 10^{-10}~Pa^{-1}$ (Browning et al., 2015), equation (7) gives a magma intrusion volume of $\Delta V_m=5.16~\Delta V$. This result falls within the range of $\Delta V_m=2~\Delta V$ to $6\Delta V$ calculated by Battaglia et al. (2008, 2019) for Mount St. Helens and Augustine volcanos, respectively. To enhance confidence, we adopt this range. Considering an accumulated volume change of $\Delta V=1.4$ to $2.1\times 10^7~m^3$ (Newman et al., 2012; Parks et al., 2012), the calculated volume of magma intrusion lies between $\Delta V_m=2.8$ to $12.6\times 10^7~m^3$. Using this value and the computed mass from equation (5), we obtain an estimated mean magma density between 2301 and 10357 kgm 3 . These high-density values indicate that the intrusion is dominated by the addition of basaltic magma.

Fig. 6 and Table 3 show that the gravity effect of the 2011-2012 Mogi source, Model 2, cannot account for all the observed gravity variations at Palea and Nea Kameni. Therefore, although magma intrusion during the unrest period in 2011-2012 is a primary process influencing the observed gravity residuals, it is not the sole process taking place within the Santorini caldera during the nearly four decades of the observation period. The 2011-2012 unrest period represents the only significant magmatic phase since the last eruption in 1950 (Parks et al., 2013). Though the calculated model for the unrest period of 2011-2012 does not fit all the temporal gravity measurements and we are lacking intermediate gravity measurements, it is imperative to account for the gravity effects during this well-established and well-measured volcanic intrusion event.

3.3.3. Model 3: Double-mogi source: 2011-2012 unrest plus a longer-term process

For Model 3, we posit the existence of a pressurized point beneath Nea Kameni, stemming from an ongoing internal process both before and after the unrest period of 2011-2012, along with the inflation source calculated for the 2011-2012 unrest. Double Mogi point sources have also been proposed by other researchers for Santorini caldera (Saltogianni and Stiros, 2013; Foumelis et al., 2013, Papageorgiou et al., 2019). To derive the optimal solution for this model, we initially fix the location of Body 1 to the mean location of the Mogi point source for the unrest period as determined by multiple researchers (Newman et al., 2012; Parks et al., 2012, 2015; Papoutsis et al., 2013; Foumelis et al.,

Table 2
Best fitted models to gravity residual (Model 1).Depth, Xo, Yo are the location of the Mogi-source point or mean location for Growth-Dg solution, given in WGS84 UTM Zone 35 coordinates, ΔM is the calculated Mass change, χ^2 is the chi-squared statistic, mean residuals are mean unexplained gravity signal from the model and Max residuals are the maximum residual at a single benchmark.

Model	Depth	Xo	Yo	ΔΜ	χ ²	Mean residuals	Max residuals
	M	m	m	Kg		μGal	μGal
Mogi-source	2182	355910	4029570	3.11 *10 ¹¹	2.18	9	40
GROWTH-dg tool	2169	355712	4030012	$4.11 *10^{11}$	1.65	14	30

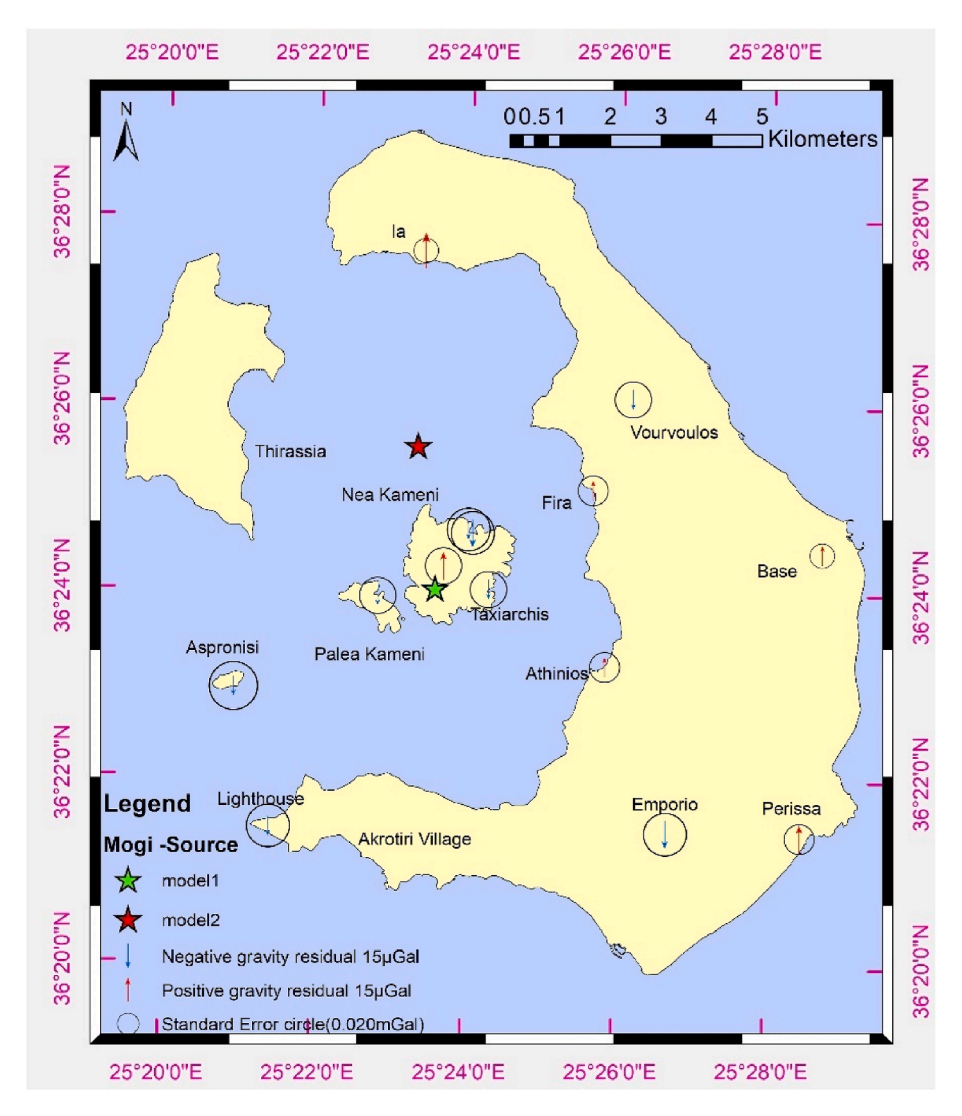


Fig. 3. Difference between the residual gravity change, $\Delta g_{residual}$, and the gravity for the best-fit Mogi point source for Model 1 (green star). The standard error circle represents the standard deviation (1 σ) of the measurements. Red star indicates Mogi-source point of Model 2.

2013). Subsequently, we conduct an inversion of gravity residuals to calculate the locations and mass intrusion of the two bodies. Employing the nonlinear inversion method described earlier, we select the solution that yields the most favorable least square differences when compared to the gravity residuals (equation (6)). Our best-fitted model is delineated in Table 4 and shown in Fig. 7.

To separate the 2011-2012 inflation source from the longer-term deformation, we correct the gravity residuals for the gravity effect of the Mogi point source of the unrest period 2011-12 using values of Body 1(Table 4) and we again employ GROWTH-dg tool to obtain the source of the gravity increase that fits the remaining residuals. The selected inversion model is presented in Fig. 8. The calculated source volume experiences a mean density increase of 45 kg/m 3 , which leads to an equivalent mass increase of 1.39x10 11 kg at a mean depth of 1354 m.

3.3.4. Evaluation of models

Model 3 appears to be a better fit to the observed gravity changes, as demonstrates by the chi-square (χ^2) statistic in Tables 2–4. However since Model 3 has more free parameters than Models 1 and 2, we utilize the F-Test for a quantitative assessment of the goodness of fit (Battaglia and Hill, 2009):

$$F_{1,3} = \frac{\left(\chi_1^2 f_1 - \chi_3^2 f_3\right) / (NP_3 - NP_1)}{\chi_3^2} \tag{8}$$

where 1, 3 indicates Models 1 and 3, respectively. The $F_{1,3}$ statistic compares the fits of Model 1 and Model 3 by taking into account the respective chi-squared value (χ^2), degrees of freedom (f), and number of parameters (NP) for each model. This statistical test assists in determining whether the improvement in fit achieved by Model 3 is statistically significant. This statistic is expected to be F-distributed with $NP_3 - NP_1$, versus f_3 degrees of freedom. The experimentally determined value of F is compared to a reference value with less than the selected probability α being exceeded by chance. If the experimental value exceeds the reference value, then there is $(1-\alpha)$ probability that the nullhypothesis (that Model 1 fits the data better than Model 3) is violated. Using the values of χ^2 from Tables 2 and 4, it is evident that $E_{\text{xperimental}} =$ 6.7 is greater than the referenced $F_{2.8} = 6.06$ from the tables (for $\alpha =$ 2.5%). Hence, Model 3 offers a superior statistical fit to the dataset. It is crucial to acknowledge that this evaluation was reliant on a limited sample of only 14 data points, raising potential questions about the reliability of the conclusions drawn from this test. Nevertheless, Model 3 remains our preferred solution because it (i) minimized the gravity residual errors; (ii) took into consideration of the 2011-12 unrest period; and (iii) is consistent with the findings of other researchers. Further supporting arguments for the selection of Model 3 are presented below.

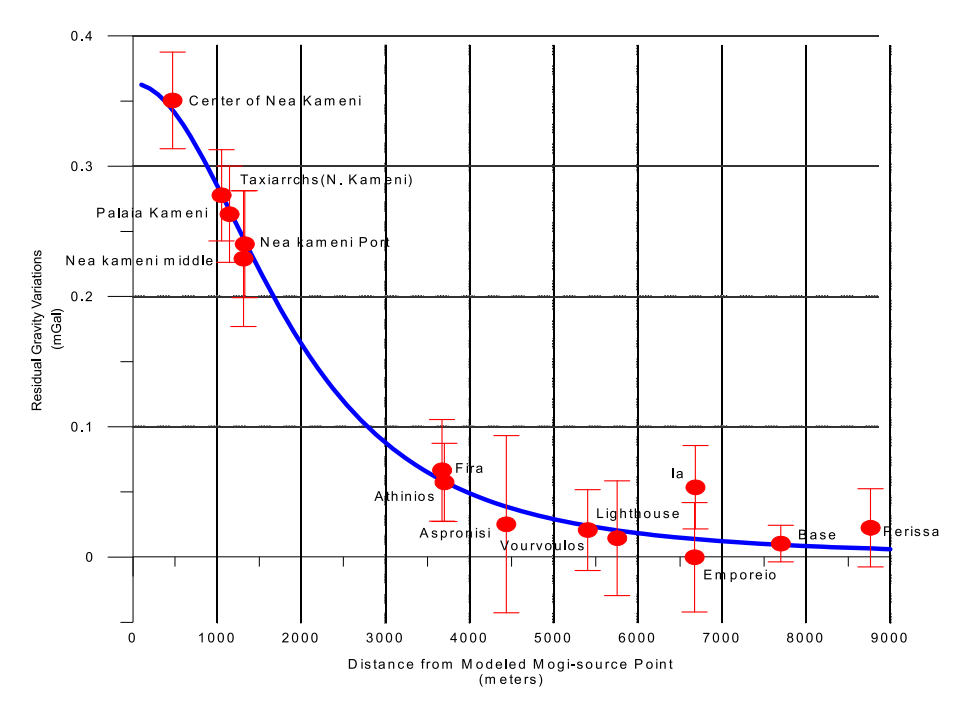


Fig. 4. Residual gravity changes, $\Delta g_{residual}$, as a function of horizontal distance from the Model 1 Mogi point source location. The blue line shows the calculated gravity effect of Model 1 (Table 2).

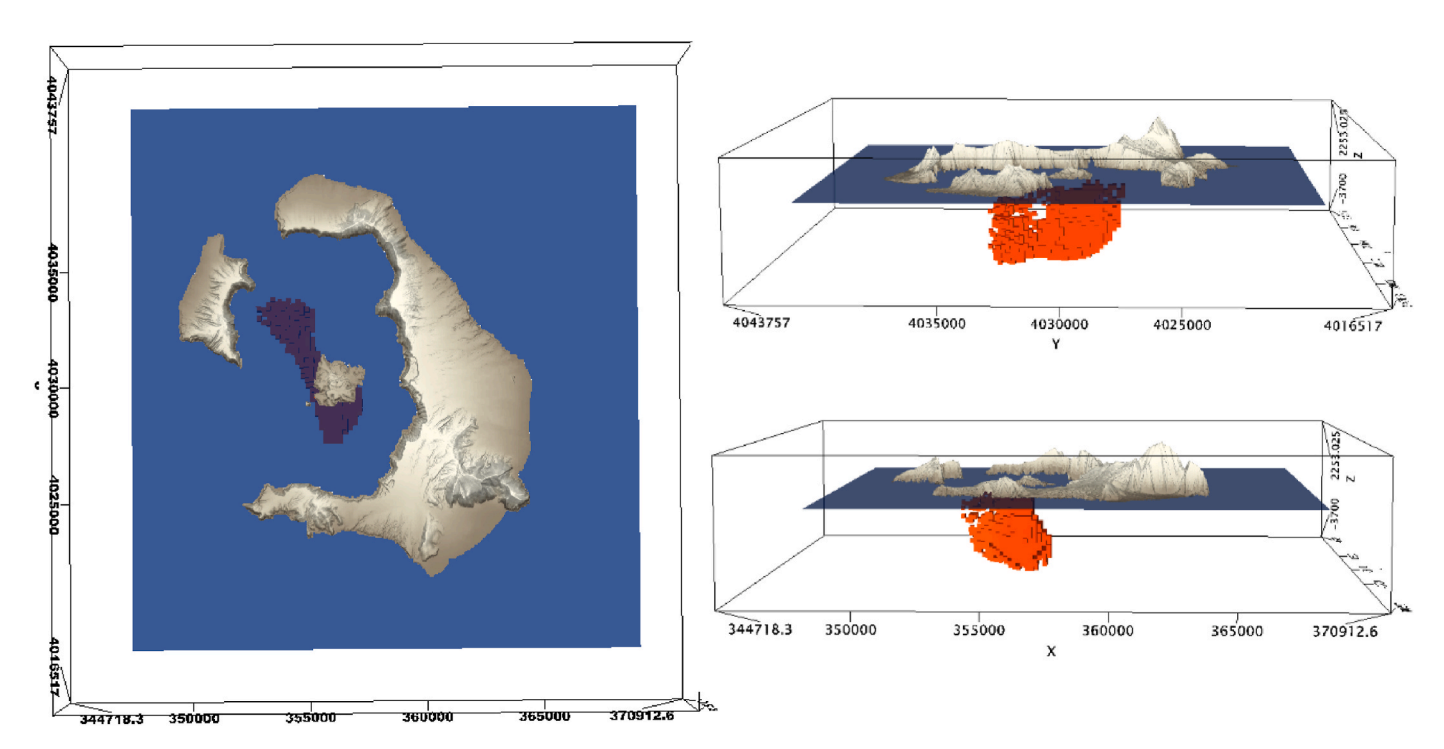


Fig. 5. Selected inversion model using GROWTH-Dg, obtained with $\lambda = 20$, reweighting (B = 2.9), and one level differential density (see Camacho et al. (2021) for details for on these parameters).

3.4. Interpretation

3.4.1. Dg/Dh gradient

When a volcanic phenomenon occurs it is accompanied by a change in mass distribution, which affects the vertical gravity gradient. Investigating changes in that gradient allows a better physical understanding and discrimination between the types of events (Rymer, 1994; Rymer and Williams-Jones, 2000; Williams-Jones and Rymer, 2002). In Fig. 9 we plot residual gravity changes versus elevation changes. There are

major dg/dh gradients at the stations Nea and Palea Kameni. Minor dg/dh gradients are recorded at Fira, Athinios, and Ia and insignificant gradients at other stations. The significant gradients fall in region II described by Gottsmann and Rymer (2002) and Brown et al. (1991), where there is an overall mass and density increase. The most likely interpretation according to Gottsmann and Rymer (2002) is magma intrusion, dyke emplacement, or a rise in the water table, that cause mass increase. While bubble resorption, bubble collapse, void filling, and hydrothermal cementation may be among the processes that result

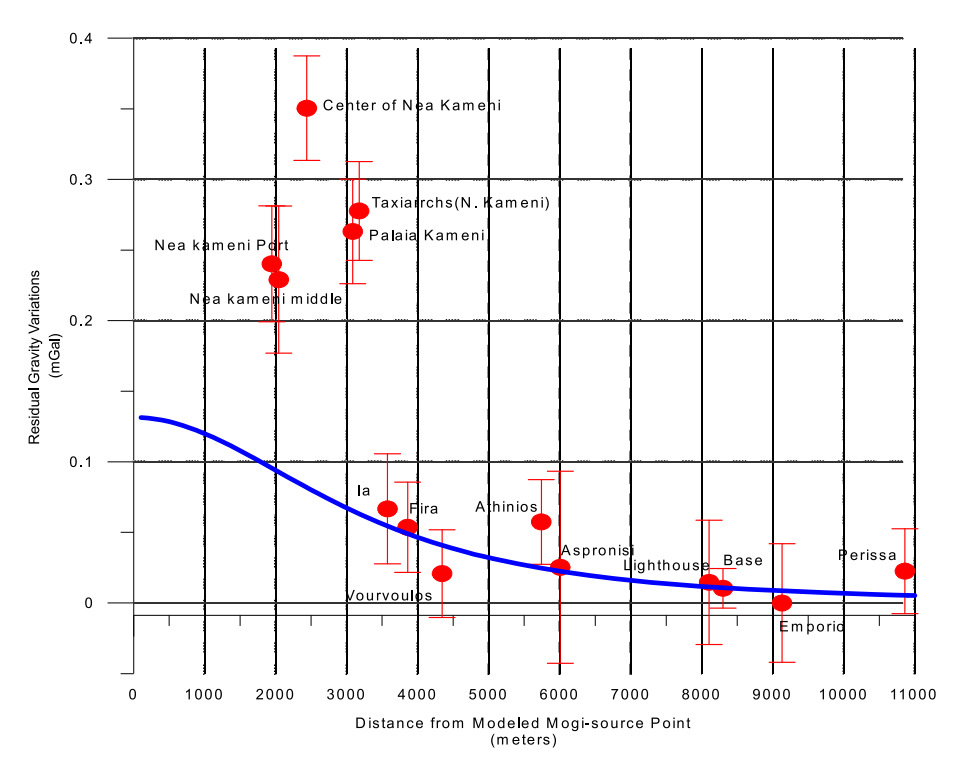


Fig. 6. Residual gravity changes compared to the gravity effect of Model 2, which is a Mogi point source fixed at the mean location and volume calculated by other researchers. The stations at plotted as a function of distance from the Mogi point source. Blue curve shows the calculated gravity effect of the Mogi point source using the maximum calculated mass intruded.

Table 3

The Mogi-source model calculated by other researchers for the 2011-12 unrest, using geodetic and remote sensing methods (Model 2).

Model	Depth	Xo	Yo	ΔM max	X^2	Mean residuals	Max residuals
Mogi-source	m 4000	M 355580	M 4032400	Kg 2.9 *10 ¹¹	140.33	μGal 75	μGal 275

Table 4
Best fitted Double Mogi-source model to gravity residual, using equation (2) (Model 3).

	Depth	Xo	Yo	ΔM	χ^2	Mean	Max residuals
						residuals	
	M	m	m	Kg*10^11		μGal	μGal
Body1	3000	355080	4031920	3.23	1.02	7	17
Body2	1350	356000	4029030	1.14			
GROWTH-dg	1354	356111	4029008	1.39	0.82	12	18

in an overall density increase (Gottsmann and Rymer, 2002). Since there are a number of potential interpretations, below we delve deeper into two specific time periods, namely the unrest period of 2011-12 and the periods before and after it.

3.4.2. Unrest period 2011-2012

The preferred Model 3, with double Mogi point sources (Table 3), has a mass increase of 3.23×10^{11} kg in Body1, with a calculated volume change, $\Delta V m$, ranging from 2.8 to 12.6×10^7 m³. These values yield an estimated density range for the intruded mass of $\rho=2564$ to 11536 kg/m³, signifying the presence of basaltic magma intrusion. While inversion models that fit geophysical data are valuable working tools, it is important to compare their results with other geophysical or geological data. This comprehensive approach allows us to gauge the credibility and reliability of the results obtained from these models.

The magma intrusion hypothesis finds additional support from various geophysical pieces of evidence. Notably, significant changes were observed in the compositions and fluxes of gas emissions from the Kameni Islands during the 2011-2012 period. Subtle increases were recorded in the diffuse flux of soil CO2, as well as in the concentrations of gases like H₂ and CH₄ in fumaroles. The ³He/⁴He ratio in fumarolic emissions also experienced alterations, indicating a convective heat pulse originating from depth, associated with the seismic activation of the NE-SW oriented Kameni fault. This convective process was attributed to the injection of new magma (Parks et al., 2013; Tassi et al., 2013; Rizzo et al., 2015; Moreira et al., 2019). Additionally, the rise of magma from depth led to elevated H2 and CO2 concentrations in the central part of the caldera (Tassi et al., 2013). Druitt et al. (2016) presented further evidence pointing towards a magmatic origin for the 2011-2012 unrest period. Additionally, Hooft et al. (2019) and McVey et al. (2020) employed 3-dimensional seismic velocity models derived from tomographic inversions of active-source P-wave travel times. These studies identified a distinct low-velocity anomaly (at least -21%) situated at depths between 2.8 km and 5 km below the northern caldera basin that

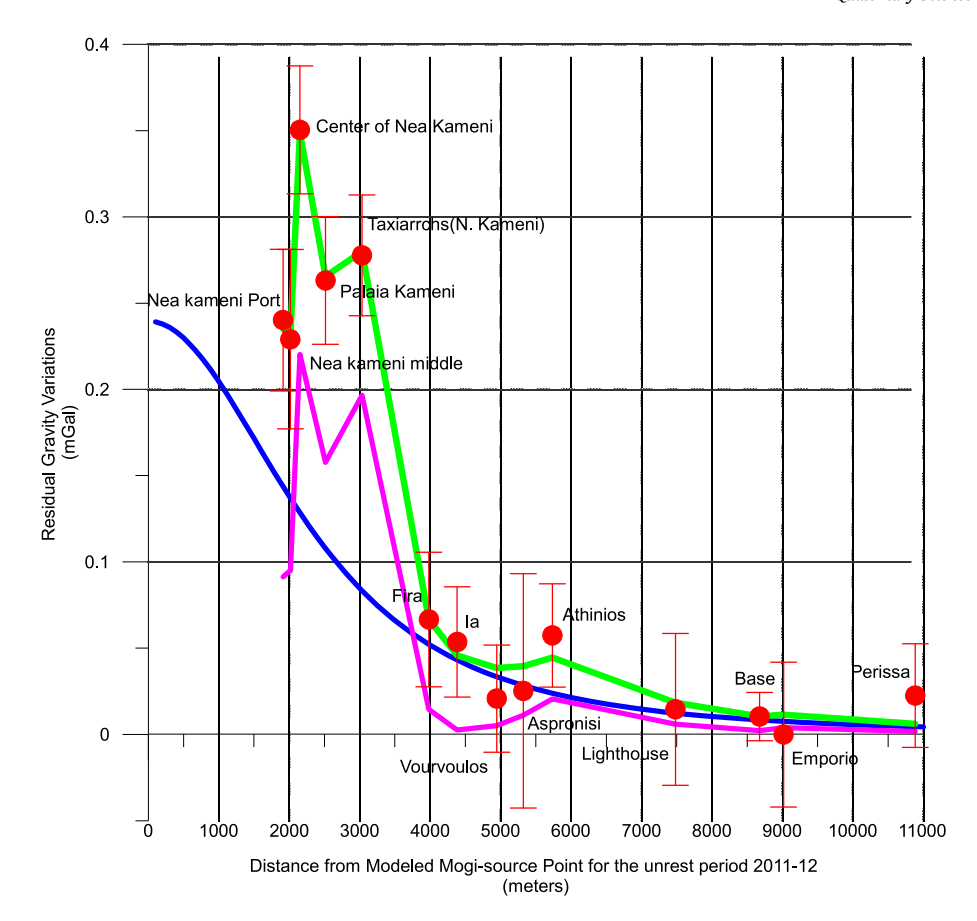


Fig. 7. Residual gravity changes for Model 3 that includes two source bodies as a function of distance from Body 1, the Mogi point source for the 2011-2012 unrest period. The blue curve shows the gravity effect of Body 1 and the purple curve shows the gravity effect of Body 2 (Table 3). The green line shows the cumulative gravity effect of the double Mogi point source in Model 3.

was interpretated as a shallow magma body causing seismic attenuation and ray bending. This anomaly aligns with the location and depth estimates of the 2011-12 inflation episode. Taken together, these lines of evidence provide strong support for the hypothesis that magma intrusion was the primary process behind the unrest observed during 2011-12. This conclusion is in line with the findings of our gravity investigation. Furthermore, our estimation of the density of the intruded magma ($\rho > 2564 \ kg/m^3$) supports the presence of basaltic magma.

3.4.3. Before and after the unrest period 2011-2012

Our results indicate the presence of an additional ongoing internal process within the caldera edifice that results in gravity increases (Fig. 6) but that occurs without observable inflation, except during the unrest period of 2011-12. Saltogianni et al. (2014) have proposed that the period of unrest during 2011-2012 marked a significant episode of deformation, characterized as the first composite pulse to induce noteworthy microseismicity and activity within the Santorini Caldera since the eruption of 1950. The ISMOSAV report (2022) highlights that following to the unrest period, the caldera regressed to a state of quiescence, exhibiting a trend akin to the pattern observed before the period of unrest. In a similar vein, Papageorgiou et al. (2019) propose that a consistent form of volcanic activity persisted at Nea Kameni both prior to, and subsequent to, the unrest episode of 2011-12. They note that this continuity in activity was unaffected by the aforementioned unrest. Given these considerations, and taking into account the absence of intermediary gravity measurements, we posit that the underlying source responsible for the gravity residuals remains unchanged both before and after the unrest period.

In our interpretation of the gravity inversion results, as depicted in Fig. 8, we have excluded the possibility of void spaces being filled with

magma. This is primarily because the sustained existence of void spaces at such shallow depths over a span of nearly 60 years is deemed improbable. Notably, the most recent volcanic eruption at Nea Kameni was in 1950. Furthermore, the concept of magma intrusion occurring at such shallow depths, either prior to or following the unrest episode of 2011-12, appears highly implausible. This assertion is rooted in the absence of corroborating evidence from other geophysical and geological indicators. For instance, there is a lack of significant seismic activity, observable inflation, or variations in the composition of fumaroles that would typically accompany such intrusive processes. Moreover, the introduction of viscous magma to passively fill pore spaces would inevitably induce substantial additional deformation, which runs contrary to the observed geodetic data. Additionally, there has been no discernible alteration in the chemical composition of both thermal gases and fluids, which might otherwise signal a form of deeper feeding process, in the period preceding the unrest episode (Arriaga and Harper, 2009). We further exclude dyke emplacement at very shallow depths. Such a process would likely alter the composition of fumaroles located beneath Nea Kameni. This perspective is at odds with the findings of the technical report by ISMOSAV (2022), which indicates that the contamination levels of fumaroles remained relatively stable both prior to, and subsequent to, the unrest episode. Additionally, supporting evidence comes from the works of Tassi et al., (2013); Parks et al., (2013), who contend that the CO2 flux emanating from Nea Kameni is predominantly of hydrothermal origin.

An increase in gravity could also be attributed to internal density changes within the volcanic system. This may result from processes such as the densification of a magma source, degassing, and vesicle collapse. Degassing of magma commonly leads to compaction and an increase in density. Notably, the gases emanating from Nea Kameni originate from a

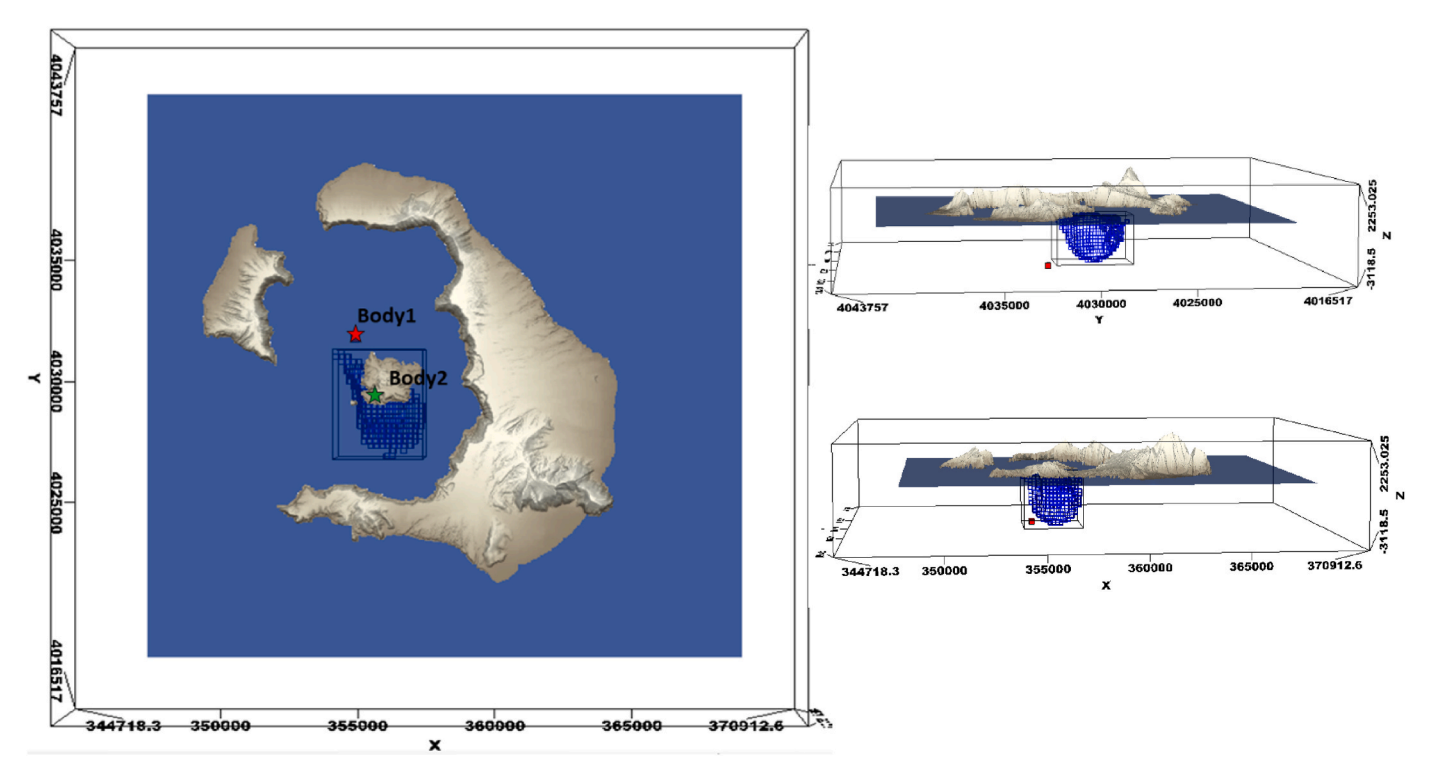


Fig. 8. Selected inversion result for Body 2 in Model 3 solved using GROWTH-Dg. This body fits the residual gravity data corrected for the predicted gravity effect of Body 1 red star), a Mogi-source for the 2011-2012 inflation episode. It was obtained with $\lambda=20$, reweighting (B = 2.9) and one level differential density (see Camacho et al. (2021) for details about these parameters). Body2 (green star) indicates Mogi-source point from Table 4.

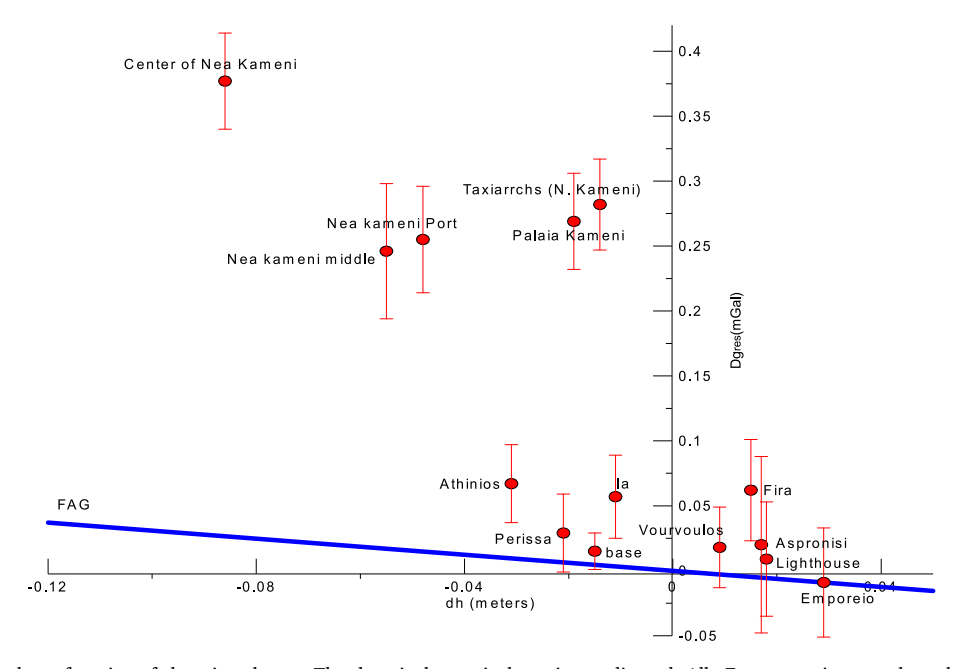


Fig. 9. The gravity residual as a function of elevation change. The slope is the vertical gravity gradient, dg/dh. For comparison we show the Free-air gradient (FAG – blue line). Errors (1σ) are presented in thin red lines for every measurement.

shallow reservoir, which undergoes degassing and has incorporated crustal materials (Moreira et al., 2019). The hydrothermal circulation facilitates the degassing of magmatic gases from the shallow chamber below Nea and Palea Kameni, although their compositions do not directly reflect the mantle source (Moreira et al., 2019; Rizzo et al., 2015).

Several researchers (Barton and Huijsmans, 1986; Higgins, 1996; Francalanci et al., 1998) have postulated the presence of a permanently

active shallow magma chamber beneath Nea Kameni. The storage of pre-eruptive magma beneath Nea Kameni has been estimated at depths ranging from 3.1 to 5 km (Barton and Huijsmans, 1986; Druitt et al., 2019). Additionally, Parks et al. (2013) demonstrated that soil gas ²²²Rn-8¹³C systematics are consistent with emissions from a largely degassed dacite under Nea Kameni. This magma chamber could continue the degassing process contributing to the observed increase in gravity over a continuous, at least 40-year, period.

Parks et al. (2015) interpreted subsidence under Nea Kameni before the unrest period of 2011-12 as the thermal cooling and the load-induced relaxation of the substrate due to lava flows emitted between 1866 and 1870. This process is not linked to a mass change, which means that gravity-height data would be expected to follow the Free Air Gravity (FAG) curve (Gostmann and Rymer, 2002). Even if we extend the stable rate for subsidence of 5-6 mma $^{-1}$ calculated from the period 1992-2010 (Foumelis et al., 2013; Papageorgiou et al., 2019) back to 1976, the resulting gravity effect (0.3086 * 0.180 = 55 μ Gal) would only account for a small portion of the observed gravity variations at the stations on the Kameni islands.

On the other hand, Foumelis et al. (2013) proposed that the deformation observed on Nea Kameni results from variations within the shallow hydrothermal system, the existence of which was reported by Fytikas et al. (1990) at depths of 800-1000 meters. These hydrothermal variations could stem from processes like density increase due to metallogenetic activities and degassing of hydrothermal fluids, or mass increase caused by a perched hydrothermal aquifer at shallow depths. Although significant variations in the water table under Nea Kameni are not reported (ISMOSAV, 2022), the precipitation of dense hydrothermal minerals, such as iron, phosphorus, manganese, and barium, near the surface can influence the gravity signal. The presence of iron-rich sediments in various bays of the Kameni Islands within the Santorini caldera, resulting from precipitation from hot submarine springs, represents a phase of late volcanic activity (Puchelt, 1973). Boström et al. (1990) also identified an active hydrothermal system with the same chemical composition as the hot springs on Nea Kameni, at depths of at least 170 meters beneath Palea Kameni. Additionally, Bostrom and Arvanitides et al. (1994) suggested an excess of hydrothermal matter containing Fe, P, Mn, and Ba in the hot springs of the caldera. They proposed that this excess material originated from a metallogenetic process within the volcano's hydrothermal system. Their work included the calculation of an annual discharge rate of nearly 105,000 kg, with an excess mean density of 500 - 1000 kg/m³, which could explain part of the observed gravity increase.

Considering the information provided, our favored interpretation involves hydrothermal variations, coupled with the phenomena of degassing and vesicle collapse taking place within the stored magma beneath the Kameni Islands.

4. Discussion

In the paragraphs above, we have presented arguments for the existence of two distinct sources that contribute to an increase in the observed gravity signal in the region, as numerically calculated in Model 3. According to this analysis, we have demonstrated a high likelihood of magma intrusion occurring at the location determined by geodetic and remote sensing (RS) methods during the 2011-12 unrest period. Additionally, we believe that both before and after the unrest, a continuous process of increasing gravity persists beneath the Kameni Islands. This phenomenon has been interpreted as a combination of hydrothermal variations, coupled with the processes of degassing and vesicle collapse within the stored magma beneath the Kameni Islands.

To arrive at Model 3, we rejected Models 1 and 2. Model 1 did not take into account the 2011-12 unrest period, resulting in a Mogi point source being inferred below the Kameni Islands, but at a greater depth than Body 2 of Model 3. Similarly, Model 2, generated based on geodetic measurements, was unable to provide a satisfactory explanation for the observed gravity variations. It is important to note that the models we have presented are simplified representations of the complex physical processes occurring within the volcanic edifice. Additionally, the significant time interval between measurements introduces the possibility of other processes that could explain the observed gravity variations or the occurrence of coupled phenomena.

Due to the limited availability of gravity data, achieving a comprehensive understanding of the volcano's behavior can be challenging.

However, measurements taken from the triangulation point on Nea Kameni since 1966 have revealed a discernible pattern of increasing gravity with decreasing rates beneath Nea Kameni (Fig. 10). Specifically, between 1966 and 1969, there was a gravity increase of 130 μ Gal (approximately 43 μ Gal/year). This trend continued with an increase of 254 μ Gal (about 36 μ Gal/year) between 1969 and 1976, followed by a slower increase of 385 μ Gal (approximately 11 μ Gal/year) from 1976 to 2012. Finally, between 2012 and 2014, a smaller increase of 24 μ Gal (around 12 μ Gal/year) was recorded. From Fig. 10, we deduce that there is an ongoing and consistent process occurring beneath Nea Kameni, which remains unaffected by the unrest period experienced during 2011-2012.

Additional measurements that align with the observed gravity residuals contribute to a more robust interpretation and reinforce our conclusions. One such set of measurements involves the flux of gases and fluid discharge. Beginning in 2002, a noticeable reduction in the volume of emitted gases from the Nea Kameni fumaroles has been documented (Arriaga and Harper, 2009; ISMOSAV, 2022). Furthermore, the discharge rates of hydrothermal fluids have shown significant decreases. Although the metallogenetic process within the shallow hydrothermal system beneath the Kameni Islands has been on the decline since 1870, Bostrom and Arvanitides et al. (1994) demonstrated that it was still ongoing in decreasing rate. In addition, the subsidence rate of Nea Kameni has exhibited a declining trend. During the pre-unrest period, the estimated subsidence from 1992 to 2010 averaged 5-6 mm per year, while the recorded subsidence from 2012 to 2017 reduced to 4-5 mm per year. These various measurements, including gas flux, fluid discharge, and subsidence rates, collectively support and reinforce the conclusions drawn from the gravity data and contribute to a more comprehensive understanding of the ongoing processes beneath the Kameni Islands.

Indeed, the decreasing rate of gravity increase, coupled with the additional measurements mentioned earlier, suggests a continuous process occurring beneath Nea Kameni both before and after the 2011-2012 unrest period. Our interpretation points primarily to a hydrothermal origin for these variations. According to the GROWTH-Dg tool solution (Fig. 5), the source of these variations is likely to be at very shallow depths, ranging from 1 to 3 km. The positive gravity residuals can be the consequence of several processes, including the density increase associated with metallogenetic activity, the degassing of hydrothermal fluids, or even the degassing and vesicle collapse of shallow stored magma beneath Nea Kameni. As the magma in the shallow chamber undergoes densification and degassing, its compressibility decreases, which could explain the decreasing rate of gravity increase observed at Nea Kameni. To gain a more comprehensive understanding of these explanations, further analysis could be conducted by establishing a denser gravity network, particularly focusing on the Kameni Islands, and incorporating shorter time intervals between repeated measurements (ranging from months to a year). This approach would enable a closer monitoring of hydrothermal circulation patterns and the effects of changes in the water table, contributing to a more precise interpretation of the ongoing processes beneath the Nea Kameni region.

5. Conclusions

Our investigation of the gravity variations in the Santorini caldera, particularly around Nea Kameni, has led to a multi-faceted understanding of the underlying processes. Using gravity inversion techniques and by considering other geological and geophysical data, we have explored different hypotheses to explain the observed gravity residuals. Our preferred interpretation, supported by a combination of gravity residuals, geodetic data, and corroborating evidence from other studies, suggests that basaltic magma intruded at the area of calculated Mogi point source during the unrest of 2011-12 and that there is also a continuous, ongoing process taking place beneath Nea Kameni. This process is most likely due to hydrothermal variations coupled with degassing and vesicle collapse occurring within the stored magma

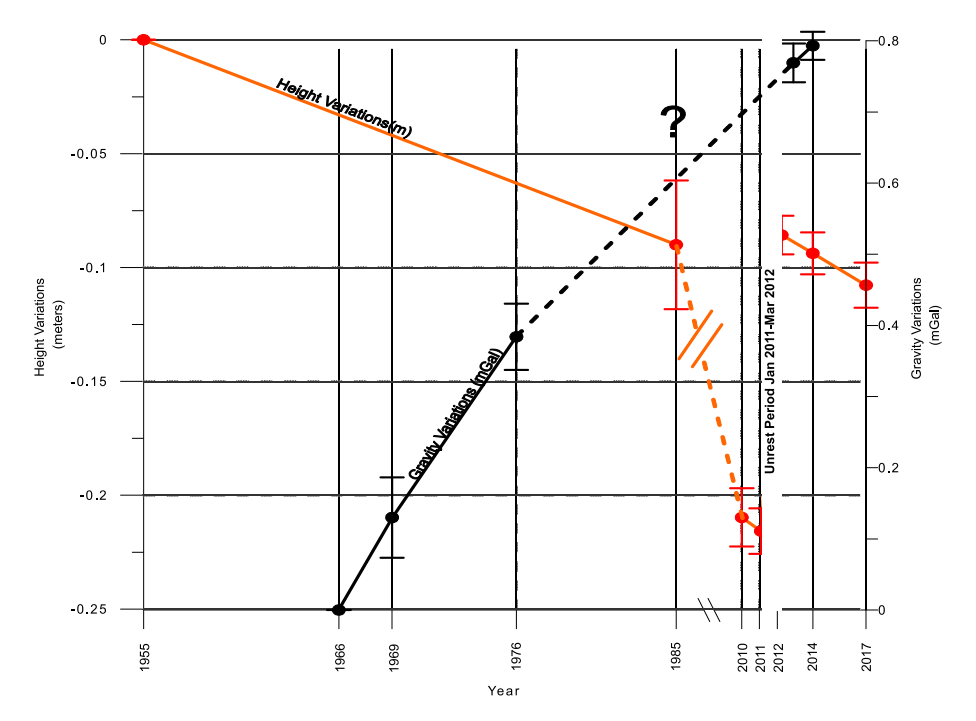


Fig. 10. Gravity variations and estimated height changes over time at the triangulation point in the center of Nea Kameni. Black symbols and line show gravity variations, while red ones show height differences. Black and red error bars present standard deviation of gravity and height, respectively.

beneath the Kameni Islands. The decreasing rate of gravity increase over time is indicative of ongoing changes in a magma chamber, possibly driven by densification and degassing. Indeed, a more comprehensive understanding of the volcanic system could be attained by implementing a denser gravity measurement network with more frequent data acquisition intervals. This would enhance our ability to capture subtle variations and monitor the evolving processes more effectively. Finally, our research highlights the complex and dynamic nature of volcanic systems. Gravity variations provide essential insights into the underlying mechanisms, but their interpretation requires integration with various other sources of data, including geophysical, geological, and geodetic information. Remote sensing tools could facilitate data collection (e.g. InSAR etc), while Geographic Information Systems (GIS) could contribute to the assimilation and analysis of the wealth of information. By combining these multidisciplinary approaches, we can gain a deeper understanding of the intricate processes taking place beneath the Santorini volcanic complex.

Declaration of competing interest

The authors declare that they have no known competing financial interests or personal relationships that could have appeared to influence the work reported in this paper.

Data availability

Data will be made available on request.

Acknowledgements

The comments and suggestions provided by Dr. Maurizio Battaglia and two other anonymous reviewers significantly improved the initial manuscript. Therefore, we kindly acknowledge their valuable contributions. EH was supported by the National Science Foundation, Division of Ocean Sciences, United States grant # 2023338.

References

Agatza –Balodimou, A.M., Papazissi, K., 1984. The gravity field of Santorini. Technica Chronica, Greece 4, 4 (in Greek language).

Anderson, K., Segall, P., 2011. Physics-based models of ground deformation and extrusion rate at effusively erupting volcanoes. J. Geophys. Res. 116, B07204 https://doi.org/10.1029/2010JB007939.

Arriaga, M.C., Harper, J.M., 2009. Geothermal Reservoirs in Volcanic Islands: the Example of Santorini. Greece.

Bagnardi, M., Poland, M.P., Carbone, D., Baker, S., Battaglia, M., Amelung, F., 2014. Gravity changes and deformation at Kilauea Volcano, Hawaii, associated with summit eruptive activity, 2009–2012. J. Geophys. Res. Solid Earth 119, 7288–7305. https://doi.org/10.1002/2014JB011506.

Barton, M., Huijsmans, J.P.P., 1986. Post-caldera dacites from the Santorini volcanic complex, Aegean Sea, Greece: an example of the eruption of lavas of near-constant composition over a 2,200 year period. Contrib. Mineral. Petrol. 94, 472–495. https://doi.org/10.1007/BF00376340.

Battaglia, M., Segall, P., Roberts, C., 2003. The mechanics of unrest at Long Valley caldera, California: 2. Constraining the nature of the source using geodetic and micro-gravity data. J. Volcanol. Geoth. Res. 127, 219–245.

Battaglia, M., Gottsmann, J., Carbone, D., Fernández, J., 2008. 4D volcano gravimetry. Geophysics 73 (6). https://doi.org/10.1190/1.2977792. WA3– WA18.

Battaglia, M., Hill, D.P., 2009. Analytical modeling of gravity changes and crustal deformation at volcanoes: the Long Valley caldera, California, case study. Tectonophysics 471, 45–57. https://doi.org/10.1016/j.tecto.2008.09.040.

Battaglia, M., Alpala, J., Alpala, R., Angarita, M., Arcos, D., Eullides, L., Euillades, P., Mueller, C., Narvaez, L., 2019. Monitoring volcanic deformation. USGS Publications Warehouse. https://doi.org/10.1016/B978-0-12-409548-9.10902-9. http://pubs.er. uses.gov/publication/70203501.

Berrino, G., Vajda, P., Zahorec, P., G Camacho, A., De Novellis, V., Carlino, S., Papčo, J., Bellucci Sessa, E., Czikhardt, R., 2022. Corrigendum: interpretation of spatiotemporal gravity changes accompanying the earthquake of 21 August 2017 on Ischia (Italy). Contrib. Geophys. Geodes. 51 (4) https://doi.org/10.31577/ congeo.2021.51.4.3.c. Jan. 2022.

Boström, K., Ingri, J., Boström, B., Andersson, P., Löfvendahl, R., 1990. Metallogenesis at Santorini: a subduction-zone related process; II, Geochemistry and origin of hydrothermal solutions on Nea Kameni, Santorini, Greece. In: Thera and the Aegean World, III: Proceedings of the Third International Congress, Santorini, Greece, 3-9 September 1989 Vol 2, Earth Sciences [Internet]. The Thera Foundation, pp. 291–299.

Boström, K., Arvanitides, N., 1994. The amount of exhalative sedimentary deposits rich in Fe. Mn. P and Ba at Santorini. Bull. Geol. Soc. Greece 30, 211–224.

Bonafede, M., Mazzanti, M., 1999. Residual gravity variations in volcanic areas: constraints to the interpretation of uplift episodes at Campi Flegrei, Italy. Phys. Chem. Earth Solid Earth Geodes. 24 (Issues 11–12), 963–967. https://doi.org/10.1016/S1464-1895(99)00143-X. ISSN 1464-1895.

Brown, G.C., Rymer, H., Stevenson, D., 1991. Volcano monitoring by microgravity and energy budget analysis. J. Geol. Soc. 148 (3), 585–593. https://doi.org/10.1144/gsjgs.148.3.0585.

- Browning, J., Drymoni, K., Gudmundsson, A., 2015. Forecasting magma-chamber rupture at Santorini volcano, Greece. Sci. Rep. 5, 15785 https://doi.org/10.1038/ srep.15785
- Cadoux, A., Scaillet, B., Druitt, T.H., Deloule, E., 2014. Magma storage conditions of large Plinian eruptions of Santorini Volcano (Greece). J. Petrol. 55, 1129–1171. https://doi.org/10.1093/petrology/egu021, 17.
- Camacho, A.G., Fernández, J., Gottsmann, J., 2011. The 3-D gravity inversion package GROWTH2.0 and its application to Tenerife Island, Spain. Comput. Geosci. 37 (Issue 4), 621–633. https://doi.org/10.1016/j.cageo.2010.12.003. ISSN 0098-3004.
- Camacho, A.G., Vajda, P., Miller, C.A., et al., 2021. A free-geometry geodynamic modelling of surface gravity changes using Growth-dg software. Sci. Rep. 11, 23442 https://doi.org/10.1038/s41598-021-02769-z.
- Carbone, D., Budetta, G., Greco, F., 2003. Possible mechanisms of magma redistribution under Mt Etna during the 1994–1999 period detected through microgravity measurements. Geophys. J. Int. 153 (Issue 1) https://doi.org/10.1046/j.1365-246X.2003.01901.x, 187–200.
- Druitt, T.H., Edwards, L., Mellors, R.M., Pyle, D.M., Sparks, R.S.J., Lanphere, M., et al., 1999. Santorini Volcano, 19. Geological Society Memoir.
- Chatzis, N., Papazachos, C., Theodoulidis, N., Hatzidimitriou, P., Vougioukalakis, G., Paulatto, M., Heath, B., Hooft, E., Toomey, D., Anthymidis, M., Ventouzi, C., 2022. Metamorphic bedrock geometry of Santorini using HVSR information and geophysical modeling of ambient noise and active-source surface-wave data. Journal of Volcanology and Geothermal Research 432, 107692. ISSN 0377-0273. https://doi.org/10.1016/j.jvolgeores.2022.107692.
- Currenti, G., 2014. Numerical evidence enabling reconciliation gravity and height changes in volcanic areas. Geophys. J. Int. 197 (1), 164–173. https://doi.org/ 10.1093/gji/ggt507. April, 2014.
- Druitt, T.H., 2014. New insights into the initiation and venting of the Bronze-Age eruption of Santorini (Greece), from component analysis. Bull. Volcanol. 794.
- Druitt, T.H., Mercier, M., Florentin, L., Deloule, E., Cluzel, N., Flaherty, T., Médard, E., Cadoux, A., 2016. Magma storage and extraction associated with plinian and interplinian activity at Santorini caldera (Greece). J. Petrol. 57 (Issue 3), 461–494. https://doi.org/10.1093/petrology/egw015.
- Druitt, Timothy H., Pyle, David M., Mather, Tamsin A., 2019. Santorini Volcano and its plumbing system. Elements 15 (3), 177–184. https://doi.org/10.2138/ gselements.15.3.177.
- Eggers, A., 1987. Residual gravity changes and eruption magnitudes. J. Volcanol. Geoth. Res. 33. 201–216. https://doi.org/10.1016/0377-0273(87)90062-X.
- Fernández, J., Rundle, J.B., 1994. Gravity changes and deformation due to a magmatic intrusion in a two-layered crustal model. J. Geophys. Res. 99 (B2), 2737–2746. https://doi.org/10.1029/93JB02449.
- Foumelis, M., Trasatti, E., Papageorgiou, E., Stramondo, S., Parcharidis, I., 2013. Monitoring Santorini volcano (Greece) breathing from space. Geophys. J. Int. 193, 161–170.
- Francalanci, L., Vougioukalakis, G., Eleftheriadis, G., Pinarelli, L., Petrone, C., Manetti, P., Christofides, G., 1998. Petrographic, chemical and isotope variations in the intracaldera post-minoan rocks of the Santorini volcanic field, Greece. In: Casale, R., Fytikas, M., Sigvaldasson, G., Vougioukalakis, G.E. (Eds.), The European Laboratory Volcanoes", Proceedings of the 2d Workshop, Santorini, Greece – 2 to 4 May 1996. EUR 18161 EN, European Commission, Luxembourg, pp. 175–186.
- Fytikas, M., Kolios, N., Vougioukalakis, G., Hardy, D.A., Keller, J., Galanopoulos, V.P., Flemming, N.C., Druitt, T.H., 1990. Post-Minoan volcanic activity of Santorini volcano. In: Volcanic Hazard and Risk, Forecasting Possibilities, Thera and the Aegean World III. The Thera Foundation, London, pp. 183–198, 2.
- Gottsmann, J., Rymer, H., 2002. Deflation during caldera unrest: constraints on subsurface processes and hazard prediction from gravity-height data. Bull. Volcanol. 64, 338–348. https://doi.org/10.1007/s00445-002-0212-7.
- Grant, F.S., West, G.F., 1965. Interpretation Theory in Applied Geophysics. McGraw-Hill, New York
- Heath, A., Davidov, E., Ford, R., Green, E.G.T., Ramos, A., Schmidt, P., 2020. Contested terrain: explaining divergent patterns of public opinion towards immigration within Europe. J. Ethnic Migrat. Stud. 46 (3), 475–488. https://doi.org/10.1080/ 1369183X.2019.1550145.
- HNMS, 2020. In: Hellenic National Meteorological Service. http://www.emy.gr/em y/el/services/paroxi-ipiresion-klimatika-dedomena, 01 Dec.
- Higgins, M.D., 1996. Magma dynamics beneath Kameni volcano, Thera, Greece, as revealed by crystal size and shape measurements. J. Volcanol. Geoth. Res. 70 (Issues 1–2), 37–48. https://doi.org/10.1016/0377-0273(95)00045-3. ISSN 0377-0273.
- Hooft, E.H., Toomey, D.R., Paulatto, M., Papazachos, C.B., Nomikou, P., Morgan, J.V., Warner, M., 2019. Seismic imaging of Santorini: subsurface constraints on caldera collapse and present-day magma recharge. Earth Planet Sci. Lett. 514, 48–61.
- ISMOSAV, 2022. Institute for the Study and Monitoring of the Santorini Volcano, Final Report of the ISMOSAV on the Monitoring of the Volcano of Santorini for the Year 2021 available at: https://www.ismosav.gr/gr/Pages/Index/22, 28/2/2023.
- Johnston, E.N., Sparks, R.S.J., Phillips, J.C., Carey, S., 2014. Revised estimates for the volume of the late Bronze Age minoan eruption, Santorini, Greece. J. Geol. Soc. 171, 583-590
- Karstens, J., Preine, J., Crutchley, G.J., Kutterolf, S., van der Bilt, W.G., Hooft, E.E., et al., 2023. Revised Minoan eruption volume as benchmark for large volcanic eruptions. Nat. Commun. 14 (1), 2497.
- Lagios, E., Sakkas, V., Novali, F., Bellotti, F., Ferretti, A., Vlachou, K., Dietrich, V., 2013. Squee SAR (TM) and GPS ground deformation monitoring of Santorini Volcano (1992- 2012): tectonic implications. Tectonophysics 594, 38–59.
- Loj, M., Porzucek, S., 2019. Detailed analysis of the gravitational effects caused by the buildings 44 in microgravity survey. Acta Geophys. 67 (6), 1799–1807.

- Mastin, L.G., 2007. A user-friendly one-dimensional model for wet volcanic plumes. Gcubed 8. https://doi.org/10.1029/2006GC001455. Q03 014.
- McVey, B.G., Hooft, E.E.E., Heath, B.A., Toomey, D.R., Paulatto, M., Morgan, J.V., Nomikou, P., Papazachos, C.B., 2020. Magma accumulation beneath Santorini volcano, Greece, from P-wave tomography. Geology 48 (3), 231–235. https://doi. org/10.1130/647127.1
- Miller, C.A., Williams-Jones, G., Fournier, D., Witter, J., 2017. 3D gravity inversion and thermodynamic modelling reveal properties of shallow silicic magma reservoir beneath Laguna del Maule, Chile. Earth Planet Sci. Lett. 459 https://doi.org/ 10.1016/j.epsl.2016.11.007, 14-27, ISSN 0012-821X.
- Mogi, K., 1958. Relations between the eruptions of various volcanoes and the deformations of the ground surface around them. Bull. Earthquake Res. Inst. Univ. Tokyo 36, 99–134.
- Moreira, M., Escartin, J., Scelin, L., Ruzie-Hamilton, L., Nomikou, P., Mevel, C., Andreani, M., 2019. New insights into the plumbing system of Santorini using helium and carbon isotopes. Geochemical Perspectives Letters 10, 46–50. https://doi.org/10.7185/geochemlet.1914.
- Naujoks, M., Kroner, C., Weise, A., Jahr, T., Krause, P., Eisner, S., 2010. Evaluating local hydrological modelling by temporal gravity observations and a gravimetric threedimensional model. Geophys. J. Int. 182 (Issue 1), 233–249. https://doi.org/ 10.1111/j.1365-246X.2010.04615.x.
- Nelder, John A., Mead, R., 1965. A simplex method for function minimization. Comput. J. 7 (4), 308–313. https://doi.org/10.1093/cominl/7.4.308.
- Newman, A.V., Stiros, S., Feng, L., Psimoulis, P., Moschas, F., Saltogianni, V., Jiang, Y., Papazachos, C., Panagiotopoulos, D.G., Karagianni, E., Vamvakaris, D., 2012. Recent geodetic unrest at Santorini caldera, Greece, geophys. Res. Lett. 39, L06309 https://doi.org/10.1029/2012GL051286.
- Nomikou, P., et al., 2014. The emergence and growth of a submarine volcano: the Kameni islands, Santorini (Greece). Geogr. Res. J. 1–2, 8–18.
- Okubo, S., Tanaka, Y., Ueki, S., et al., 2013. Gravity variation around Shinmoe-dake volcano from February 2011 through March 2012—results of continuous absolute gravity observation and repeated hybrid gravity measurements. Earth Planets Space 65, 563–571. https://doi.org/10.5047/eps.2013.03.014.
- Panagiotopoulos, D.G., Papazachos, C., Vougioukalakis, G., Stiros, S.C., Laopoulos, Th, Fytikas, M., Karagianni, E., Vamvakaris, D., Mochas, F., Saltogianni, V., Albanakis, K., 2015. Santorini Volcano: the Intra-caldera Unrest of the Period of 2011-2012,as Revealed by Seismicity, Temperature, Sea-Level, Geochemical and GPS Data. AUT, Thessaloniki, pp. 1–997, 2014.
- Papageorgiou, E., Foumelis, M., Trasatti, E., Ventura, G., Raucoules, D., Mouratidis, A., 2019. Multi-sensor SAR geodetic imaging and modelling of Santorini volcano postunrest response. Rem. Sens. 11, 259.
- Papoutsis, I., Papanikolaou, X., Floyd, M., Ji, K.H., Kontoes, C., Paradissis, D., Zacharis, V., 2013. Mapping inflation at Santorini volcano, Greece, using GPS and InSAR. Geophys. Res. Lett. 40 (2), 267–272. Foumelis et al 2013.
- Paraskevas, M., Paradeisis, D., Kolovos, I., Nomikou, P., Papanikolaou, D., Raptakis, C., 2014. Tectonic structure of Santorini volcanic field based on terrestrial gravity measurements, 1976–2012. In: MESONISOS 1st International Geo-Cultural Symposium. MESONISOS, Santorini, p. 16, 6–8 Jun 2014.
- Paraskevas, M., Paradissis, D., Raptakis, C., Nomikou, P., Hooft, E., Papanikolaou, D., 2019. Geodetic and Geophysical Approach of the Gravitational Field in Santorini Volcanic Group, Conference. May 2019. JISDM 2019 At, Athens, Greece. https://doi. org/10.13140/RG.2.2.15196.03209.
- Paraskevas, M., Paradissis, D., Raptakis, C., Nomikou, P., Hooft, E., Bejelou, K., 2021. Gravity observations on Santorini island (Greece): historical and recent campaigns. Contrib. Geophys. Geodes. 51, 24. https://doi.org/10.31577/congeo.2021.51.1.1.
- Paraskevas, M., Papadopoulos, N., Kagiadakis, V., 2022. Geoid model determination for the hellenic territory "HELLAS GEOID, 2022". In: HMGS Technical Report, Available in. https://www.gys.gr/hmgs-bulletin_en.html, 10.13140/RG.2.2.22830.38721. (in Greek Language).
- Paraskevas, M., Papadopoulos, N., Ampatzidis, D., 2023. Geoid model determination for the hellenic area "hellas geoid 2023.". Acta Geod Geophys. https://doi.org/ 10.1007/s40328-023-00416-9.
- Parks, M.M., Biggs, J., England, P., Mather, T.A., Nomikou, P., Palamartchouk, K., Papanikolaou, X., Paradissis, D., Parsons, B., Pyle, D.M., Raptakis, C., Zacharis, V., 2012. Evolution of Santorini volcano dominated by episodic and rapid fluxes of melt from depth. Nat. Geosci. 5, 749–754.
- Parks, M.M., Caliro, S., Chiodini, G., Pyle, D.M., Mather, T.A., Berlo, K., Edmonds, M., Biggs, J., Nomikou, P., Raptakis, C., 2013. Distinguishing contributions to diffuse CO2 emissions in volcanic areas from magmatic degassing and thermal decarbonation using soil gas 222Rn-8 13C systematics: application to Santorini volcano, Greece. Earth Planet Sci. Lett. 377–378, 180–190.
- Parks, M.M., Moore, J., Papanikolaou, X., Biggs, J., Mather, T.A., Pyle, D.M., Raptakis, C., Paradissis, D., Hooper, A., Parsons, B., Nomikou, P., 2015. From quiescence to unrest - 20 years of satellite geodetic measurements at Santorini volcano, Greece. J. Geophys. Res. 120, 1309–1328. https://doi.org/10.1002/ 2014.JR011540
- Puchelt, H., 1973. Recent iron sediment formation at the Kameni islands, Santorini (Greece). In: Amstutz, G.C., Bernard, A.J. (Eds.), Ores in Sediments. International Union of Geological Sciences. Springer, Berlin, Heidelberg. https://doi.org/ 10.1007/978-3-642-65329-2_18, 3.
- Pyle, D.M., Elliott, J.R., 2006. Quantitative morphology, recent evolution and future activity of the Kameni islands volcano. Santorini, Greece, Geosphere 2, 253–268.
- Rizzo, A.L., Barberi, F., Carapezza, M.L., Piazza, A. Di, Francalanci, L., Sortino, F., D'Alessandro, W., 2015. New mafic magma refilling a quiescent volcano: evidence from He-Ne-Ar isotopes during the 2011–2012 unrest at Santorini, Greece. G-cubed 16, 798–814. https://doi.org/10.1002/2014GC005653.

- Rymer, H., 1994. Microgravity changes as a precursor to volcanic activity. J. Volcanol. Geoth. Res. 61, 311–329.
- Rymer, H., Williams-Jones, G., 2000. Volcanic eruption prediction: magma chamber physics from gravity and deformation measurements. Geophys. Res. Lett. 27 (16), 2389–2392. https://doi.org/10.1029/1999GL011293.
- Saltogianni, V., Stiros, S., 2013. A new algorithm for modelling simple and double Mogi magma sources in active volcanoes: accuracy, sensitivity, limitations and implications. Bull. Volcanol. 75 (10), 1–14.
- Saltogianni, V., Stiros, S.C., Newman, A.V., Flanagan, K., Moschas, F., 2014. Time-space modeling of the dynamics of Santorini volcano (Greece) during the 2011–2012 unrest. J. Geophys. Res. Solid Earth 119.
- Sonker, I., Tripathi, J.N., 2022. Swarnim, Remote sensing and GIS-based landslide susceptibility mapping using frequency ratio method in Sikkim Himalaya. Quaternary Science Advances 8, 100067. https://doi.org/10.1016/j. qsa.2022.100067. ISSN 2666-0334.
- Seigel, H.O., 1995. A Guide to High Precision Land Gravimeter Surveys. Scintrex Ltd.,
- Sharma, P.V., 1986. Geophysical Methods in Geology. Elsevier, New York.
- Sigurdsson, H., et al., 2006. Marine investigations of Greece's Santorini volcanic field. Eos Trans. AGU 87 (34), 337–342. https://doi.org/10.1029/2006EO340001.
- Sparks, R.S.J., Wilson, C.J.N., 1990. The minoan deposits: a review of their characteristics and interpretation. In: Hardy, D.A. (Ed.), Thera and the Aegean World III.2. The Thera Foundation, London, pp. 89–99.
- Tassi, F., Vaselli, O., Papazachos, C.B., Giannini, L., Chiodini, G., Vougioukalakis, G.E., Karagianni, E., Vamvakaris, D., Panagiotopoulos, D., 2013. Geochemical and isotopic changes in the fumarolic and submerged gas discharges during the 2011-2012 unrest at Santorini caldera (Greece). Bull. Volcanol. 75, 711. https://doi.org/10.1007/s00445-013-0711-8.
- Taloor, A.K., Adimalla, N., Goswami, A., 2021. Remote sensing and GIS applications in geoscience. Applied Computing and Geosciences 11, 100065. https://doi.org/ 10.1016/j.acags.2021.100065. ISSN 2590-1974.

- Taloor, A.K., Kothyari, G.C., Goswami, A., Mishra, A., 2022. Geospatial technology applications in quaternary science. Quaternary Science Advances 7, 100059. https://doi.org/10.1016/j.qsa.2022.100059. ISSN 2666-0334.
- Taloor, A.K., Dumka, R.K., Kothyari, G.C., Neloy Khare, P.S., 2023. Active tectonics and surface processes using geospatial technology. J. Appl. Geophys. 215, 105140 https://doi.org/10.1016/j.jappgeo.2023.105140. ISSN 0926-9851.
- Torge, W., 1989. Gravimetry. de Gruyter, Berlin-New York, 1989.
- Vajda, Peter, 2016. Recent Developments and Trends in Volcano Gravimetry. https://doi.org/10.5772/63420.
- Vajda, P., Zahorec, P., Bilčík, D., Papčo, J., 2019. Deformation induced topographic effects in interpretation of spatiotemporal gravity changes: review of approaches and new insights. In: Surveys in Geophysics. https://doi.org/10.1007/s10712-019-09547-7
- Vajda, P., Zahorec, P., Miller, C.A., Le Mével, H., Papčo, J., Camacho, A.G., 2021. Application of deformation-induced topographic effect in interpretation of 2013–2016 spatiotemporal gravity changes at Laguna del Maule (Chile), 2021, online, 19–30 Apr 2021 EGU General Assembly. https://doi.org/10.5194/ egusphere-egu21-467. EGU21-467.
- Vajda, P., Camacho, A.G., Fernández, J., 2022. Benefits and Limitations of the Growth Inversion Approach in Volcano Gravimetry Demonstrated on the Revisited 2004–2005 Tenerife Unrest. Surv Geophys. https://doi.org/10.1007/s10712-022-00738.0
- Walsh, J.B., Rice, J.R., 1979. Local changes in gravity resulting from deformation.
 J. Geophys. Res. 84, 165–170. https://doi.org/10.1029/JB084iB01p00165.
- Williams-Jones, G., Rymer, H., 2002. Detecting volcanic eruption precursors: a new method using gravity and deformation measurements. J. Volcanol. Geoth. Res. 113 (Issues 3-4), 379–389. https://doi.org/10.1016/S0377-0273(01)00272-4. ISSN 0377-0273.
- Yokoyama, I., Tajima, H., 1957. A gravity survey on volcano mihara, ooshima island by means of a worden gravimeter. Bull. Earthq. Res. Inst. 35, 23–33.